

Received December 3, 2019, accepted December 16, 2019, date of publication December 24, 2019, date of current version January 3, 2020.

Digital Object Identifier 10.1109/ACCESS.2019.2961977

# Energy Efficiency Characterization in Heterogeneous IoT System With UAV Swarms Based on Wireless Power Transfer

YUANYUAN YAO<sup>ID1</sup>, (Member, IEEE), ZHENGYU ZHU<sup>ID2,3</sup>, (Member, IEEE),  
SAI HUANG<sup>ID4</sup>, (Member, IEEE), XINWEI YUE<sup>ID1</sup>, (Member, IEEE),  
CHUNYU PAN<sup>ID1</sup>, (Member, IEEE), AND XUEHUA LI<sup>ID1</sup>

<sup>1</sup>School of Information and Communication Engineering, Beijing Information Science and Technology University, Beijing 100101, China

<sup>2</sup>School of Information Engineering, Zhengzhou University, Zhengzhou 450001, China

<sup>3</sup>Zhengzhou University Research Institute of Industrial Technology Company, Ltd., Zhengzhou 450001, China

<sup>4</sup>Key Laboratory of Universal Wireless Communications, Ministry of Education, Beijing University of Posts and Telecommunications, Beijing 100876, China

Corresponding authors: Sai Huang (huangsai@bupt.edu.cn) and Zhengyu Zhu (zhuzhengyu6@gmail.com)

This work was supported in part by the Natural Science Foundation of Beijing Municipality under Grant 19L2022, Grant 4202046, Grant 4204099, and Grant KZ201911232046, in part by the National Natural Science Foundation of China under Grant 61801052 and Grant 61801434, in part by the Science and technology Project of Beijing Municipal Education Commission under Grant KM202011232002 and KM202011232003, in part by the Key Research and Cultivation Project at Beijing Information Science and Technology University under Grant 5211910926 and Grant 5211910924, in part by the Supplementary and Supportive Project for Teachers at Beijing Information Science and Technology University under Grant 5029011103 and Grant 5111911147, in part by the Zhengzhou Municipal Science Technology Innovation Project under Grant 2019CXZX0037, in part by the China Postdoctoral Science Foundation under Grant 2018M642784, in part by the Scientific and Technological Key Project of Henan Province under Grant 192102310178, and in part by the Key Laboratory of Dynamic Cognitive System of Electromagnetic Spectrum Space (Nanjing Univ. Aeronaut. Astronaut.), Ministry of Industry and Information Technology under Grant KF20181901.

**ABSTRACT** An unmanned aerial vehicle (UAV) swarm together with a large-scale heterogeneous Internet of Things (IoT) network consisting of macrocells and energy-constrained IoT transmitters (IoT-Ts) is investigated. The UAVs are utilized as flying robot swarms that intelligently transfer energy to the energy-constrained IoT-Ts on the ground. Each IoT-T has an associated IoT device (IoT-D) that is placed at a fixed distance in a random direction. The transmission probability of the energy-constrained IoT-Ts is derived by considering one-slot charging and two-slot charging according to three dimensional (3D) locations, respectively. The coverage probability of each type of IoT-D is investigated. The energy efficiency is derived by considering the transmission power of the active IoT-Ts and the effect of the association biasing factor, and the energy efficiency is also maximized by deploying the optimal density of IoT-Ts. Simulation results are examined to validate the accuracy of our theoretical analysis. Results illustrate the insightful effects of the network parameters, and the helpful guidelines for practical UAV swarms and IoT system design.

**INDEX TERMS** Unmanned aerial vehicle swarms, heterogeneous IoT networks, wireless power transfer, stochastic geometry, energy efficiency.

## I. INTRODUCTION

With the development of the fifth generation wireless communication technology, the Internet of Things (IoT) system has recently been integrated widely into the field of wireless communications [1]–[3]. The IoT aims to provide the interconnection of all objects anytime and anywhere [4].

The associate editor coordinating the review of this manuscript and approving it for publication was Jinming Wen<sup>ID</sup>.

Typically, IoT systems consist of small, energy-constrained nodes, and these nodes cannot continue working for a long periods of time and at long distances [5]. In some special scenarios, such as forest fire warning and pipeline inspection, the batteries of these IoT nodes cannot be manually replaced or recharged; thus the system performance is limited due to the energy constraints of the IoT device [6].

The development of unmanned aerial vehicle (UAV) swarms is recognized as an innovative approach to

complement existing IoT networks [7]–[10]. The introduction of UAV swarms has several advantages compared with traditional wireless networks on the ground. First, they can be quickly deployed and configured [11], and transfer energy to the IoT nodes in some special scenarios on the ground; Second, they are highly controllable and have low-cost features [12]; Moreover, with the high probability of enjoying a line-of-sight (LoS) link, UAV swarms can have a relatively good channel state to complete wireless power transfer [13]. Terrestrial IoT nodes can transmit/receive data by using the harvested power, and the system can be named as a UAV-assisted wireless powered heterogeneous IoT network.

For terrestrial heterogeneous IoT networks, the dimension of energy should be considered, from which the heterogeneous IoT network faces certain challenges, such as supporting high network throughput, high energy efficiency, and good quality-of-service requirement. The macrocells together with multi-tier IoT transmitters (IoT-Ts) are considered as a key technology to overcome these challenges for future wireless networks. IoT-Ts have small coverage area and require low transmission power, making them suitable for deployment in the special areas [6]. Therefore, the density of the IoT-Ts and the transmission power should be considered to improve the energy efficiency of the heterogeneous IoT system.

#### A. RELATED WORK

Wireless power transfer (WPT) recently received considerable attention for recharging devices because of the large-scale wireless IoT nodes in the IoT system. It enables the IoT nodes to collect energy from the radio-frequency (RF) of the surrounding transmitters, which is beneficial to prolong the period of manual battery replacement, and effectively saves energy cost [14]–[17]. The feasibility of WPT and the wireless powered communication network (WPCN) have been investigated in the recent works [18]–[20]. However, the number of IoT sensor nodes is large in some special scenarios, such as forest fire warning and pipeline inspection. These nodes are always distributed in a wide area, making it difficult to deploy a swarm of power beacons for transferring energy to the energy-constrained IoT nodes. Thus, charging the batteries of the IoT nodes remains an urgent problem. The UAV with energy harvesting can be viewed as a key solution to overcome these problems [21].

The research on UAV-enabled wireless powered heterogeneous IoT network is still in the preliminary stage, and most existing works focus on studying a single UAV that transmits energy to terrestrial IoT-Ds [22]–[24]. Huang *et al.* in [6] investigate a joint optimization of power allocation and trajectory design of a single UAV to provide infrastructure-less IoT services. The objective is to maximize the minimum energy harvested by the large-scale terrestrial distributed IoT nodes. Xu *et al.* in [25] investigate a UAV transferring energy to the terrestrial devices.

In [26], a novel method of swarm robot task planning based on UAV and ground coordination is proposed for emergency

rescue. The UAV swarms employ a decentralized method to deploy the searching paths on the basis of the location information. Liu *et al.* in [27] propose that using the tools of stochastic geometry [28], [29], the UAV swarms can be modeled as homogeneous Poisson point processes (HPPPs) in 3D space. However, the detailed derivation process is not illustrated with stochastic geometry. Although some works are related to the UAV swarms and ground wireless networking, few studies considered the UAV swarm-assisted wireless powered large-scale heterogeneous IoT network and applied stochastic geometry to 3D analysis. Most related works ignore the impact of air-ground energy transmission from UAV swarms to IoT nodes in the system.

This study considers a UAV-assisted heterogeneous IoT system consisting of a swarm of UAVs, a tier of macro base stations (MBSs), and multi-tier of heterogeneous IoT systems. The UAVs are utilized as flying robot swarms that intelligently transfer energy to the energy-constrained IoT-Ts on the ground, when the energy-constrained IoT-Ts are located inside an energy harvesting zone. Each energy-constrained IoT-T has an associated IoT-D located at a specific distance in a random direction. The two types of IoT-D in the system are as follows: 1) the associated IoT-Ds that the associated IoT-Ts are active (have a communication request) and 2) the associated IoT-Ds that have a communication request, and the associated IoT-Ts are inactive, together with the ordinary IoT-Ds requiring communications. The transmission probability of the energy-constrained IoT-Ts is derived by considering one-slot and two-slot charging, respectively. The coverage probabilities of every type of IoT-Ds are analyzed and derived, the network throughput and energy efficiency are both characterized by considering the effect of the IoT-T density, the association biasing factor, and the transmission power of the active IoT-Ts. The numerical results and simulations are examined to provide insightful guideline on the various system parameters for the design in practice.

The main contributions of this work are summarized as follows:

- 1) We propose a UAV-assisted heterogeneous IoT system; The UAV swarms intelligently transfer energy to the energy-constrained IoT-Ts on the ground, and evaluate the transmission probability of the energy-constrained IoT-Ts with different cases;
- 2) We consider the impact of the density of the UAV swarms and the transmission power of the IoT-Ts on the activity of the IoT-Ts in each tier;
- 3) We analyze the energy efficiency by considering the effect of the IoT-T density and the association biasing factor. The energy efficiency is also maximized by deploying the optimal density of IoT-Ts.

The remainder of this paper is organized as follows. Section II describes the system model and performance metrics. The transmission probability of the IoT-Ts is investigated in Section III. Coverage probability of the two types of users are presented in Section IV. Section V studies the network throughput and the energy efficiency. Numerical results and

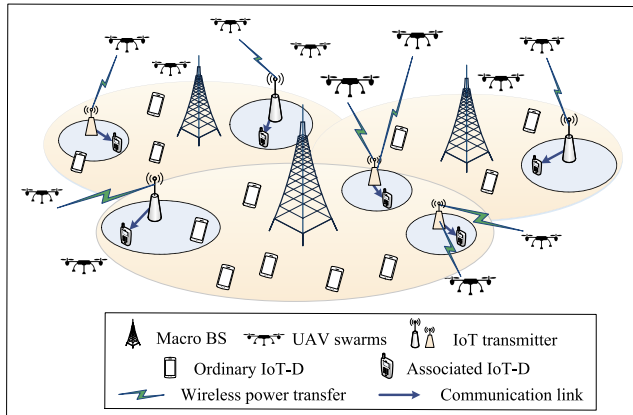


**FIGURE 1.** An illustration of heterogeneous IoT network.

simulations are conducted in Section VI. Finally, Section VII concludes the paper.

*Notations:* Throughout this paper, we use  $\mathbb{E}[\cdot]$  to denote the expectation operator.  $\Pr(\cdot)$  stands for the abbreviation for probability.

## II. SYSTEM MODEL

### A. NETWORK MODEL

Let us consider a UAV-assisted downlink heterogeneous IoT system, as shown in Fig. 1, which is composed of a swarm of UAVs and a large-scale HetNet that consists of a tier of MBSs, denoted by tier 0, along with  $K$  tiers of energy-constrained IoT-Ts, denoted by  $\mathcal{K} = \{1 \dots K\}$ . The UAVs are utilized as flying robot swarms that intelligently transfer energy to the energy-constrained IoT-Ts on the ground. Moreover, the UAVs are distributed according to a HPPP  $\Phi_u$  with density  $\mu_u$ , and have a fixed transmission power  $P_u$  and a single antenna. It is noted that we assume the UAVs are deployed at a fixed altitude  $h_{uav}$  for avoiding the frequent ascending or descending caused by diverse terrains.

On the other hand, All the MBSs and the energy-constrained IoT-Ts in the same tier are assumed to be deployed according to independent HPPPs  $\Phi_m$  and  $\Phi_k$ , with density  $\mu_m$  and  $\mu_k$ ,  $k \in \mathcal{K}$ , ( $\mu_m \ll \mu_k$ ). Each energy-constrained IoT-T in tier  $k$  supports its transmission solely with RF energy harvesting from the UAVs, and has its associated IoT-D to serve primarily, each associated IoT-D is located at a distance of  $d_{a,k}$  away in a random direction, and the associated IoT-Ds in tier  $k$  follow a HPPP with density  $\mu_k$ . Time is partitioned into slots with unit duration. In each time slot, an energy-constrained IoT-T in tier  $k$  becomes active only when 1) its associated IoT-D has a communication request; 2) the battery of the energy-constrained IoT-T is fully charged by the flying UAVs. We further assume that MBSs consume power from the grid, and use the same power  $P_m$  for data transmissions. When the batteries are fully charged, the energy-constrained IoT-Ts transmits signal with the maximum power, and the maximum transmit power in the tier  $k$  is  $P_k$ . Moreover, it is noted that  $P_m \gg P_k$ .

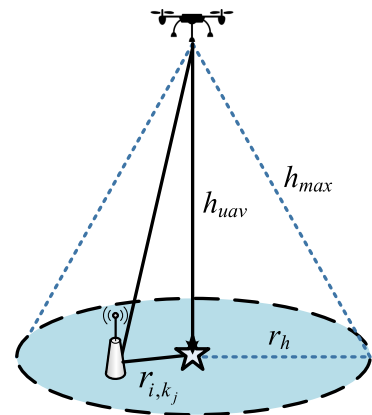


**FIGURE 2.** Harvesting zone of the UAV.

The ordinary IoT-D are geographically situated according to a HPPP with density  $\mu_o$ . Hence, the users in the heterogeneous IoT network can be classified in two types: the associated IoT-Ds are preferentially served by their own IoT-Ts; the ordinary IoT-Ds can be served by any MBSs or active IoT-Ts. All the IoT-Ds have a communication request with probability  $\omega_{req}$ .

Each UAV in the swarms is assumed to be associated with a 3D cone which is named as harvesting zone to delivers RF energy to the energy-constrained IoT-T, as shown in Fig. 2,  $h_{max}$  is defined as the busbar which is the maximum distance of the harvesting zone from the UAV to the energy-constrained IoT-T. The dotted line on the ground is the bottom of the harvesting zone which is a disk with radius  $r_h$ , where  $h_{max}^2 = h_{uav}^2 + r_h^2$ , and the five-pointed star representing the UAV is the vertical mapping from the air to the ground. Therefore, the horizontal distance between the  $i$ -th UAV to the  $j$ -th IoT-T in tier  $k$  on the horizontal plane, is equivalent to the distance between the five-pointed star to the IoT-T, which is denoted by  $r_{i,k_j}$  in Fig. 2. For the simplicity of theoretical analysis, we refer to “cone bottom” as “harvesting zone” in the sequel.

### B. AIR TO GROUND CHANNEL MODEL

As discussed in [30], the energy-constrained IoT-Ts on the ground receive two groups of signals experiencing the line-of-sight (LoS) and non-line of sight (NLoS). Due to the different occurrence probabilities of LoS or NLoS links, the channel power gain from the  $i$ -th UAV to the  $j$ -th IoT-T in tier  $k$  is written as

$$g_{i,k_j} = \begin{cases} h_{i,k_j}^{-\alpha} & \text{LoS}, \\ \chi h_{i,k_j}^{-\alpha} & \text{NLoS}, \end{cases} \quad (1)$$

where

$$h_{i,k_j} = \sqrt{(x_{u,i} - x_{k_j})^2 + (y_{u,i} - y_{k_j})^2 + h_{uav}^2}. \quad (2)$$

Each UAV  $i \in \Phi_u$  has a 3D coordinate, that is  $(x_{u,i}, y_{u,i}, h_{uav})$ . Each energy-constrained IoT-T  $j \in \Phi_k$  has a 2D coordinate on the horizontal plane, that is  $(x_{k_j}, y_{k_j})$ .

Therefore, the distance between the  $i$ -th UAV to the  $j$ -th IoT-T in tier  $k$  on the horizontal plane can be given by  $r_{i,k_j} = \sqrt{(x_{u,i} - x_{k_j})^2 + (y_{u,i} - y_{k_j})^2}$ , which is shown in Fig. 2.  $\chi$  is the additional loss to the free space propagation loss which is caused by the NLoS link, and  $\alpha$  is the air-to-ground path loss exponent.

It is worth highlighting that the probability of receiving LoS and NLoS groups is vastly higher than that of multipath fading [5]. Therefore, the impact of multipath fading is neglected. The probability of having LoS connections is dependent on the propagation environment and the elevation angle  $\theta$ , i.e., the sight of the IoT-T to the UAV, which is given by  $\theta_i = \tan^{-1} \left( \frac{h_{uav}}{\sqrt{r_{i,k_j}^2 + h_{uav}^2}} \right)$ .

The probability of the LoS connections with an elevation angle  $\theta_i$  can be approximated to a simple modified Sigmoid function (S-curve), which is given by

$$\Pr(LoS, \theta_i) = \frac{1}{1 + \varsigma \exp(-\beta [\theta_i - \varsigma])}, \quad (3)$$

where  $\varsigma$  and  $\beta$  are S-curve parameters and related to the propagation environment (woods, rural, dense urban, etc.). Accordingly, the NLoS probability are linked as

$$\Pr(NLoS, \theta_i) = 1 - \Pr(LoS, \theta_i). \quad (4)$$

Finally, the channel power gain from the  $i$ -th UAV to the  $j$ -th IoT-T in tier  $k$  can be written as

$$g_{i,k_j} = \Pr(LoS, \theta_i) \times \left( \sqrt{r_{i,k_j}^2 + h_{uav}^2} \right)^{-\alpha} + \Pr(NLoS, \theta_i) \times \chi \left( \sqrt{r_{i,k_j}^2 + h_{uav}^2} \right)^{-\alpha}. \quad (5)$$

### C. ENERGY HARVESTING MODEL

The RF energy harvester in each energy-constrained IoT-T is deployed with a power converting module, which transforms the energy of the RF signals received from the UAVs into direct current (DC) power. Such module in reality have certain sensitivity requirements, such as the harvested power should be larger than a predefined threshold, so that the energy harvesting module can receive energy efficiently. Thus, the harvesting zone is defined. As mentioned in Section II-A and Fig. 2, we have defined the harvesting zone as a disk with radius  $r_h$  centered at each mapping node of the UAV (the five-pointed star in Fig. 2).

Accordingly, an energy-constrained IoT-T can harvest RF energy from its nearest UAV supposing it is located in the UAV's harvesting zone. Otherwise, the power harvested by an energy-constrained IoT-T located outside any harvesting zone is too small to trigger the energy harvesting module, and is assumed to be neglected. Similar with [31], it is assumed that the harvesting zones of different UAVs do not overlap most of the time. The probability that an energy-constrained IoT-T located in a harvesting zone is denoted by  $\omega_h$ . Therefore, we have

$$\omega_h = 1 - e^{-\pi r_h^2 \mu_u}. \quad (6)$$

As shown in Fig. 2, the distance between an energy-constrained IoT-T and its nearest UAV is denoted as  $h_{i,k_j} = \sqrt{r_{i,k_j}^2 + h_{uav}^2}$ , where  $r_{i,k_j} \leq r_h$ . Therefore, the average energy harvested by an energy-constrained IoT-T in a time slot is denoted as

$$P_{slot} = \eta P_u g_{i,k_j} \\ = \eta P_u \left( \Pr(LoS, \theta) \times h_{i,k_j}^{-\alpha} + \Pr(NLoS, \theta) \times \chi h_{i,k_j}^{-\alpha} \right), \quad (7)$$

where  $\eta$  ( $0 < \eta < 1$ ) is the harvesting efficiency.

At each time slot, an energy-constrained IoT-T becomes active only when 1) its associated IoT-D has a communication request, the probability is denoted as  $\omega_{req}$ ; 2) the battery of the energy-constrained IoT-T is fully charged by the flying UAVs, the probability is denoted as  $\omega_t$ . As the point process of the UAVs  $\Phi_u$  changed independently over different time slots, the events that an energy-constrained IoT-T has been fully charged in one slot, and that its associated IoT-D has a communication request in next time slot are independent. Consequently, the active probability of the IoT-Ts denoted by  $\omega_f$  is given by

$$\omega_f = \omega_{req} \cdot \omega_t. \quad (8)$$

The calculation of  $\omega_f$  will be derived in Section III.

Similar to the assumptions in [32], we assume that the MBSs and the active IoT-Ts in tier  $k$ ,  $k \in (0 \cup \mathcal{K})$ , are distributed according to a new HPPP  $\tilde{\Phi}_k$  with density

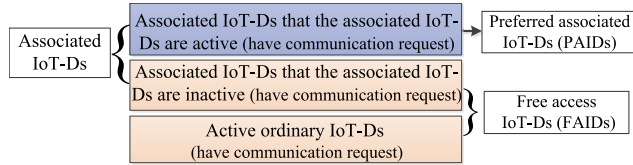
$$\mu_k^{(a)} = \begin{cases} \omega_t \times \mu_k, & k \in \mathcal{K}, \\ \mu_m, & k = 0. \end{cases} \quad (9)$$

### D. CELL ASSOCIATION

By the thinning property [33], the associated IoT-Ds that have communication request in tier  $k$  follow a HPPP with density  $\omega_{req} \cdot \mu_k$ ; and the ordinary IoT-Ds that have communication request follow a HPPP with density  $\omega_{req} \cdot \mu_o$ ; respectively. With the above analysis, as seen in Fig. 3, the associated IoT-Ds that have communication request are divided into two categories: some of them are served by their own associated IoT-Ts; the remaining IoT-Ds are served by other active IoT-Ts or MBSs since their associated IoT-Ts are inactive. Therefore, the locations of the two type of the associated IoT-Ds that have communication request in tier  $k$  are subject to two HPPPs with density  $\omega_f \cdot \omega_{req} \mu_k$  and  $(1 - \omega_f) \cdot \omega_{req} \mu_k$ . The associated IoT-Ds (have communication request) that are served by their own IoT-Ts are referred to as preferred associated IoT-Ds (PAIDs), the remaining IoT-Ds that have communication request are referred to as free access IoT-Ds (FAIDs). All the FAIDs can be modeled by a HPPP with density

$$\tilde{\mu}_o = \sum_{k=1}^K (1 - \omega_f) \cdot \omega_{req} \mu_k + \omega_{req} \cdot \mu_o. \quad (10)$$

We consider a cell association scheme with a biasing factor  $\mathcal{A}_k$  ( $\mathcal{A}_k > 0$ ), where increasing  $\mathcal{A}_k$  means the MBSs or the

**FIGURE 3.** Two types of IoT-Ds.

active IoT-Ts in tier  $k$  will effectively serve more FAIDs and offload more data from other tiers, and is named by cell range expansion [34]. When  $\mathcal{A}_k = 1$ , the FAIDs are connected to the MBSs or the active IoT-Ts in tier  $k$  with the largest receive power. Following [35], we have the following Lemma.

*Lemma 1:* The probability that a typical FAID connects to a MBSs or a tier- $k$  IoT-T is

$$\Pi_k = \frac{\mu_k^{(a)} (P_k \mathcal{A}_k)^{\frac{2}{\alpha}}}{\sum_{i=0}^K \mu_i^{(a)} (P_i \mathcal{A}_i)^{\frac{2}{\alpha}}}, \quad k \in (0 \cup \mathcal{K}), \quad (11)$$

where  $P_k = P_m$ , when  $k = 0$ .

Let  $X_k$  denote the distance between the typical FAID and its serving MBS or IoT-T in tier  $k$ . The PDF of the distance  $X_k$  is given as follows [36]

*Lemma 2:* The PDF  $s_{X_k}(x)$  of the distance  $X_k$  between the FAID and its serving MBS or IoT-T in tier  $k$  is

$$s_{X_k}(x) = \frac{2\pi\mu_k^{(a)}}{\Pi_k} x \exp\left(-\pi \sum_{i=0}^K \mu_i^{(a)} \left(\frac{P_i \mathcal{A}_i}{P_k \mathcal{A}_k}\right)^{\frac{2}{\alpha}} x^2\right). \quad (12)$$

Note that the total interference of a typical FAID received is from all IoT-Ts or MBSs in tier  $i$  which are located out of a circle centered at the typical FAID with radius  $d_j = x \left(\frac{P_i \mathcal{A}_i}{P_k \mathcal{A}_k}\right)^{-\alpha}$ .

Denote the random variable  $num_k$  as the number of FAIDs associated with a typical MBS or IoT-T in tier  $k$ , the probability mass function (pmf) of  $num_k$  is given by [33],

$$\begin{aligned} s_{num_k}(n) &= \Pr\{num_k = n\} \\ &= \frac{3.5^{3.5} \Gamma(n+3.5)}{\Gamma(3.5) n!} \left(\frac{\tilde{\mu}_o \Pi_k}{\mu_k^{(a)}}\right)^n \left(3.5 + \frac{\tilde{\mu}_o \Pi_k}{\mu_k^{(a)}}\right)^{-(n+3.5)}. \end{aligned} \quad (13)$$

It is worth highlighting if any FAID is connected to a MBS, then the MBS is active, i. e., the MBS transmits signal and consumes energy, which is given by  $1 - s_{num_0}(0)$ . Accordingly, the transmitting MBSs form a new HPPP with density  $\tilde{\mu}_m = \mu_m (1 - s_{num_0}(0))$ , where

$$s_{num_0}(0) = \left(1 + \frac{\tilde{\mu}_o \Pi_k}{3.5 \mu_k^{(a)}}\right)^{-3.5}, \quad k = 0. \quad (14)$$

Based on the above analysis, the locations of the active MBSs and IoT-Ts in tier  $k$  can be re-modeled as a HPPP  $\tilde{\Phi}_k^{(a)}$

with density,

$$\tilde{\mu}_k^{(a)} = \begin{cases} \omega_t \times \mu_k, & k \in \mathcal{K}, \\ \tilde{\mu}_m = \mu_m (1 - s_{num_0}(0)), & k = 0. \end{cases} \quad (15)$$

In addition, if the association biasing factor  $\mathcal{A}_k$  in tier  $k$  is larger than that in tier 0, more FAIDs will connect to the IoT-Ts, thus resulting in a smaller  $\tilde{\mu}_0^{(a)}$  and allowing more MBSs to get into the sleep mode.

## E. PERFORMANCE METRICS

In this paper, we utilize the following metrics to evaluate the performance.

### 1) COVERAGE PROBABILITY

The coverage probability is defined as the probability that a randomly selected IoT-D that has communication request can successfully receive data at its target rate. Specifically, given the total bandwidth  $W$ , the number of requesting IoT-Ds that connected to a MBS or IoT-T  $N$ , the signal-to-interference ratio (SIR), and a corresponding target  $\mathcal{T}$ , the coverage probability is given by

$$\Psi = \Pr\left\{\frac{W}{N} \log_2(1 + SIR) \geq \mathcal{T}\right\}. \quad (16)$$

### 2) ENERGY EFFICIENCY

The energy efficiency is the amount of data that can be transmitted successfully to the IoT-Ds of all tiers with unit power, which is measured by bps/Joule. Let the total energy consumption denote as  $Q_c$ , the network throughput is denoted as  $C_t$ , the energy efficiency is given by

$$\mathcal{H}_c = \frac{C_t}{Q_c} = \frac{\sum \mu \cdot \Psi \cdot \mathcal{T}}{Q_c}. \quad (17)$$

The symbols and notations utilized in the paper are listed in Table 1.

## III. TRANSMISSION PROBABILITY OF THE IoT-TS

From (8), the transmission probability of the IoT-Ts  $\omega_t$  depends on  $\omega_f$  and  $\omega_{req}$ . In this section,  $\omega_f$  will be derived using the Markov chain (MC) model. For convenience, we assume that the active IoT-Ts will transmit all the stored energy in one time slot, and we focus the mapping node of a typical UAV on the ground at the origin, as shown in Fig. 2, from (7), when the IoT-T is located at the edge of a harvesting zone, the harvested power from the typical UAV is minimized, which can be expressed as

$$P_{slot}^{\min} = \eta P_u \times \left(\sqrt{r_h^2 + h_{uav}^2}\right)^{-\alpha} \times \gamma, \quad (18)$$

where  $\gamma = (\Pr(LoS, \theta) + \chi \Pr(NLoS, \theta))$ , and  $P_{slot}^{\min} \leq P_{slot}$ . Therefore, the battery of an energy-constrained IoT in tier  $k$ ,  $k \in (0 \cup \mathcal{K})$ , can be fully charged during one time slot if  $0 \leq P_k \leq P_{slot}^{\min}$ , which is named as *one-slot charging*. In the same way, if  $P_{slot}^{\min} < P_k \leq 2 P_{slot}^{\min}$ , the battery is fully charged within at most two time slots, this case is named as

**TABLE 1.** Symbol notations.

Symbol	Definition
$\mu_u$	Density of the UAVs
$P_u$	Transmission power of the UAVs
$h_{uav}$	Vertical height of the UAVs
$\mu_m, \mu_k$	Density of the MBSs and the energy-constrained IoT-Ts in tier $k$
$P_m, P_k$	Transmission power of the MBSs and IoT-Ts in tier $k$
$d_{a,k}$	Fixed distance of an IoT-T in tier $k$ to its associated IoT-D
$\alpha$	Path-loss exponent
$\omega_{req}$	Communication request probability of an IoT-T
$g_{x,y}$	The channel power gain from node $x$ to node $y$
$\eta$	Energy harvesting efficiency
$\mu_o$	Density of the ordinary IoT-D
$\mathcal{A}_k$	Association biasing factor of tier- $k$
$\Pi_k$	The probability that a typical FAID connects to a MBSs or a tier- $k$ IoT-T
$\tilde{\mu}_k^{(a)}$	Density of the active MBSs and IoT-Ts in tier $k$
$\tilde{\mu}_o$	Density of the FAIDs
$\Psi$	Coverage probability
$C_t$	Network Throughput
$Q_c$	Total energy consumption
$\mathcal{H}_c$	Energy efficiency

*two-slot charging*. Hence, the transmission probability of the IoT-Ts  $\omega_t$  can be derived. However, if  $P_k > 2 P_{slot}^{\min}$ , the case is called *multi-slot charging*, which is out of the scope of this paper. Since most of the derivations in this part follow a similar derivation method with that in [31], we omit the detailed proofs of the propositions in the sequel.

#### A. ONE-SLOT CHARGING

If  $0 \leq P_k \leq P_{slot}^{\min}$ , the battery is fully charged within one time slot. Thus the power condition of the IoT-Ts can be marked as two grade {0, 1}, which are corresponding to the power level 0 and  $P_k$ , respectively. Thus, the state transition probability matrix denoted as  $\mathbf{M}_1$  is given by

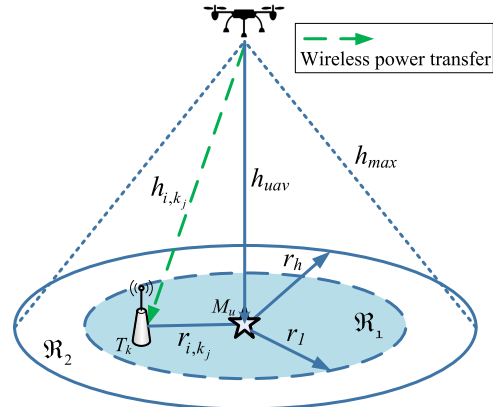
$$\mathbf{M}_1 = \begin{bmatrix} 1 - \omega_h & \omega_h \\ \omega_{req} & 1 - \omega_{req} \end{bmatrix}. \quad (19)$$

Therefore,  $\omega_t$  is obtained from the steady-state convergence theorem of MC, as given in the following proposition.

*Proposition 1:* If  $0 \leq P_k \leq P_{slot}^{\min}$ , the transmission probability of a typical IoT-T in tier  $k$  is

$$\begin{aligned} \omega_t = \omega_f \omega_{req} &= \frac{\omega_h}{\omega_h + \omega_{req}} \omega_{req} \\ &= \frac{1 - e^{-\pi r_h^2 \mu_u}}{1 - e^{-\pi r_h^2 \mu_u} + \omega_{req}} \omega_{req}. \end{aligned} \quad (20)$$

From (20), it can be observed that the transmission probability of a typical IoT-Ts in tier  $k$  depends on  $\mu_u$ ,  $r_h$ , and  $\omega_{req}$ , but has no dependence on  $P_k$ . This is due to that once an IoT-Ts located inside a harvesting zone, it can be ensured to be fully charged within one time slot under the proposed condition  $0 \leq P_k \leq P_{slot}^{\min}$ , with  $\omega_f = \frac{\omega_h}{\omega_h + \omega_{req}}$ .

**FIGURE 4.** The partitioned harvesting zone of two-slot charging.

#### B. TWO-SLOT CHARGING

If  $P_{slot}^{\min} < P_k \leq 2 P_{slot}^{\min}$ , the battery is fully charged within at most two time slots. As shown in Fig. 4, the harvesting zone is divided into two regions,  $\mathfrak{R}_1$  and  $\mathfrak{R}_2$ , respectively. Let the node  $M_u$  denote a typical UAV that mapping on the ground; and  $T_k$  denote a typical energy harvesting IoT-T in tier  $k$ .  $\mathfrak{R}_1$  is a circle centered at  $M_u$  with radius  $r_1$ , and  $\mathfrak{R}_2$  is an annulus centered at  $M_u$  with radii  $0 < r_1 < r_h$ .

It is assumed that when the IoT-T in tier  $k$  is located at the edge of the range  $\mathfrak{R}_1$ , it can just be exactly fully charged, thus we have

$$P_k = \eta P_u \times \left( \sqrt{r_1^2 + h_{uav}^2} \right)^{-\alpha} \times \gamma, \quad (21)$$

$r_1$  can be derive from (21) as

$$r_1 = \sqrt{\left( \frac{P_k}{\eta P_u \gamma} \right)^{-\frac{2}{\alpha}} - h_{uav}^2}. \quad (22)$$

The average power harvested by  $T_k$  from the nearest UAV in one slot is shown in (7). If  $T_k$  is located in the region  $\mathfrak{R}_1$ , it can be fully charged; else if  $T_k$  is located inside the region  $\mathfrak{R}_2$ , it will be charged to a range  $[0.5P_k, P_k]$ .

Thus the power condition of the IoT-Ts can be marked as three grade {0, 1, 2}, which are corresponding to the power level  $[0, 0.5P_k]$ ,  $[0.5P_k, P_k]$  and  $P_k$ , respectively. Thus, the state transition probability matrix denoted as  $\mathbf{M}_2$  is given by

$$\mathbf{M}_2 = \begin{bmatrix} 1 - \omega_h & \omega_h - \omega_1 & \omega_1 \\ 0 & 1 - \omega_h & \omega_h \\ \omega_{req} & 0 & 1 - \omega_{req} \end{bmatrix} \quad (23)$$

The probability of  $\omega_1$  is derived similarly with (6) as

$$\begin{aligned} \omega_1 &= 1 - e^{-\pi r_1^2 \mu_u} \\ &= 1 - e^{-\pi \left( \left( \frac{P_k}{\eta P_u \gamma} \right)^{-\frac{2}{\alpha}} - h_{uav}^2 \right) \mu_u}. \end{aligned} \quad (24)$$

*Proposition 2:* If  $P_{slot}^{\min} < P_k \leq 2P_{slot}^{\min}$ , the transmission probability of a typical IoT-T in tier  $k$  is

$$\begin{aligned}\omega_t &= \omega_f \omega_{req} \\ &= \frac{\omega_h}{\omega_h + \omega_{req} \left( \frac{2\omega_h - \omega_1}{\omega_h} \right)} \omega_{req}. \end{aligned}\quad (25)$$

It is worth highlighting from (25) that,  $\omega_t$  is a decreasing function of  $P_k$  as  $r_1$  is a decreasing function. The reason is that increasing  $P_k$  resulting to a smaller region  $\mathfrak{R}_1$ , which means that most of the IoT-Ts need to be fully charged within two time slots, i.e., the probability  $\omega_f$  becomes smaller. Hence, the transmission probability of a typical IoT-T in tier  $k$ ,  $\omega_t$  becomes smaller.

#### IV. COVERAGE PROBABILITY

In this section, we derive the coverage probability of both the PAIDs and FAIDs. Note that the PAIDs are served by their associated IoT-Ts, and FAIDs can be served by the MBSs or the active IoT-Ts. Therefore, we compute the coverage probability of the PAIDs and FAIDs separately.

##### A. COVERAGE PROBABILITY OF THE PAIDS

In a large-scale heterogeneous IoT system, compared to the aggregated interference, the thermal noise is always be neglected [34]. Therefore, we investigate the SIR by considering that all MBSs and the active IoT-Ts coexist on the frequency spectrum. The received SIR of a typical PAIDs that located at  $x_0$  and served by its associated IoT-T in tier- $k$  located at  $y_{k,0}$  is written as

$$SIR_k^{PAID} = \frac{P_k g_{x_0, y_{k,0}} d_{a,k}^{-\alpha}}{\sum_{j=0}^K \sum_{i \in \tilde{\Phi}_j^{(a)} \setminus y_{k,0}} P_j g_{x_0, y_{j,i}} \|y_{j,i} - x_0\|^{-\alpha}}. \quad (26)$$

From (16), the condition coverage probability of a PAIDs that is served by its associated IoT-T in tier- $k$  is

$$\begin{aligned}\Psi_{cov,k}^{PAID} &= \Pr \left\{ \frac{W_k}{1 + num_k} \log_2 \left( 1 + SIR_k^{PAID} \right) \geq \mathcal{T}_t^{PAID} \right\} \\ &= \mathbb{E} \left[ \Pr \left( SIR_k^{PAID} \geq \Xi_t^{PAID} (num_k) \right) | num_k \right], \end{aligned}\quad (27)$$

where  $\Xi_t^{PAID} (num_k) = 2^{\frac{(1+num_k)\mathcal{T}_t^{PAID}}{W_k}} - 1$ ,  $\mathcal{T}_t^{PAID}$  is the target SIR,  $W_k$  is the total available bandwidth. It is worth noting that  $W_k$  is divided by the associated PAID and some FAIDs connected to the corresponding IoT-T in tier  $k$ . By assuming that the number of the IoT-Ds,  $num_k$ , and  $SIR_k^{PAID}$  are independent, the coverage probability can be obtained in Result 1 as follows.

*Result 1:* The coverage probability of a PAIDs that is served by its associated IoT-T in tier- $k$  is

$$\begin{aligned}\Psi_{cov,k}^{PAID} &= \sum_{n=0}^{\infty} \exp \left( - \sum_{j=0}^K \tilde{\mu}_j^{(a)} \left( 2^{\frac{(1+num_k)\mathcal{T}_t^{PAID}}{W_k}} - 1 \right)^{\frac{2}{\alpha}} \right. \\ &\quad \times d_{a,k}^2 \kappa(\alpha) \left( \frac{P_j}{P_k} \right)^{\frac{2}{\alpha}} \left. \right) s_{num_k}(n), \end{aligned}\quad (28)$$

where  $\kappa(\alpha) = \pi \Gamma \left( 1 + \frac{2}{\alpha} \right) \Gamma \left( 1 - \frac{2}{\alpha} \right)$ , and  $\alpha > 2$  with  $\Gamma(x) = \int_0^\infty t^{x-1} e^{-t} dt$  indicating the Gamma function, and  $s_{num_k}(n)$  in given in (13).

*Proof:* See Appendix A.  $\square$

##### B. COVERAGE PROBABILITY OF THE FAIDS

We consider the coverage probability of the FAIDs that are randomly located in the heterogeneous IoT system, which can be either an associated IoT-D whose associated IoT-T is not active or an ordinary IoT-D, and are served by MBSs or active IoT-Ts. Since a typical FAID can associate with only one tier, the coverage probability that a typical FAIDs connects with the  $k^{th}$  tier is obtained as

$$\begin{aligned}\Psi_{cov,k}^{FAID} &= \Pr \left\{ \frac{W_k}{1_{\{k \in 0 \cup \mathcal{K}\}} + num_k} \log_2 \left( 1 + SIR_k^{FAID} \right) \geq \mathcal{T}_t^{FAID} \right\} \\ &= \mathbb{E} \left[ \Pr \left( SIR_k^{FAID} \geq \Xi_t^{FAID} (num_k) \right) | num_k \right], \end{aligned}\quad (29)$$

where  $\Xi_t^{FAID} (num_k) = 2^{\frac{(1_{\{k \in 0 \cup \mathcal{K}\}} + num_k)\mathcal{T}_t^{FAID}}{W_k}} - 1$ ,  $\mathcal{T}_t^{FAID}$  is the target SIR. Different with (27), the total bandwidth is divided by  $1_{\{k \in 0 \cup \mathcal{K}\}} + num_k$ , for  $k = 0$ , it is  $num_k$ , and for  $k \in \mathcal{K}$ , it is  $(num_k + 1)$ .  $SIR_k^{FAID}$  is the SIR at the typical FAID (located at  $x'_0$ ) at a distance  $x$  from the connected MBS or IoT-T in tier  $k$  (located at  $y'_{k,0}$ ), which is denoted as

$$SIR_k^{FAID} = \frac{P_k g_{x'_0, y'_{k,0}} x^{-\alpha}}{\sum_{j=0}^K \sum_{i \in \tilde{\Phi}_j^{(a)} \setminus y'_{k,0}} P_j g_{x'_0, y'_{j,i}} \|y'_{j,i} - x'_0\|^{-\alpha}}, \quad (30)$$

where  $g_{x'_0, y'_{k,0}}$  is the channel power gain from the link  $x'_0$  to  $y'_{k,0}$ .  $x$  is the distance between the node  $x'_0$  and  $y'_{k,0}$ . Then We have the following Result 2 as follows.

*Result 2:* The coverage probability that a typical FAIDs connects with the  $k^{th}$  tier is,

$$\begin{aligned}\Psi_{cov,k}^{FAID} &= \sum_{n=1}^{\infty} s_{num_k}(n) \left[ \int_0^\infty 2\pi x \frac{\sum_{i=0}^K \mu_i^{(a)} (P_i A_i)^{\frac{2}{\alpha}}}{(P_k A_k)^{\frac{2}{\alpha}}} \right. \\ &\quad \times \exp \left( -\pi x^2 \sum_{j=0}^K \tilde{\mu}_j^{(a)} \left( \frac{P_j}{P_k} \right)^{\frac{2}{\alpha}} \mathcal{M} \left( \Xi_t^{FAID} (num_k), \alpha, \frac{A_j}{A_k} \right) \right) \\ &\quad \left. \times \exp \left( -\pi \sum_{j=0}^K \mu_j^{(a)} \left( \frac{P_j A_j}{P_k A_k} \right)^{\frac{2}{\alpha}} x^2 \right) dx \right], \end{aligned}\quad (31)$$

where

$$\begin{aligned} \mathcal{M}\left(\Xi_t^{FAID}(num_k), \alpha, \frac{\mathcal{A}_j}{\mathcal{A}_k}\right) \\ = \frac{2\Xi_t^{FAID}(num_k)\left(\frac{\mathcal{A}_j}{\mathcal{A}_k}\right)^{\left(\frac{2}{\alpha}-1\right)}}{\alpha-2} \\ \times {}_2F_1\left[1, 1-\frac{2}{\alpha}; 2-\frac{2}{\alpha}; -\Xi_t^{FAID}(num_k)\frac{\mathcal{A}_k}{\mathcal{A}_j}\right], \quad (32) \end{aligned}$$

and  ${}_2F_1[., .; .; .]$  is the Gauss hypergeometric function [33].

*Proof:* See Appendix B.  $\square$

## V. ENERGY EFFICIENCY

The network throughput is defined as the total amount of the signal that is successfully received by the PAIDs and the FAIDs, from the expressions in (11), (28), and (31). The network throughput can be obtained as

$$\begin{aligned} C_t = \mathcal{T}_t^{PAID} \sum_{k=1}^K \omega_t \mu_k \Psi_{cov,k}^{PAID} + \mathcal{T}_t^{FAID} \sum_{k=0}^K \Psi_{cov,k}^{FAID} \Pi_k \\ \times \left( \sum_{k=1}^K (1 - \omega_f) \cdot \omega_{req} \mu_k + \omega_{req} \cdot \mu_o \right). \quad (33) \end{aligned}$$

The total energy consumption of the network includes the power transmitted by the active MBSs, and the power of the active IoT-Ts which is transmitted by the UAVs. Note that the energy for the operations during the sleep mode and the circuit power is not considered in this work due to that they are relatively small. Thus the total energy consumption can be denoted as

$$Q_c = \mu_m (1 - s_{num_0}(0)) P_m + \omega_t \cdot \mu_1 P_1. \quad (34)$$

For different tier of the active IoT-Ds (PAIDs and FAIDs, and  $k \in \mathcal{K}$ ), we assume the target rate thresholds are unified as  $\mathcal{T}_t$ . Using the definition of (17), we have the following Result.

*Result 3: The explicit solution of the energy efficiency is given by (35), as shown at the bottom of this page.*

for the convenience of analysis, we consider a two-tier IoT network on the ground with one tier of MBSs,  $k = 0$ , and one tier of energy-constrained IoT-Ts,  $k = 1$ . For the

energy efficiency expression in (35), we take a average load approximation, where the number of IoT-Ds served by a MBS or an active IoT-T, which is denoted as  $num_k$ , is approximated by its mean value

$$\mathbb{E}[num_k] = \frac{\tilde{\mu}_o \Pi_k}{\tilde{\mu}_k^{(a)}}, \quad (36)$$

and we assume that  $\Pr(num_k = \mathbb{E}[num_k]) = 1$ . In this case, the energy efficiency in Result 3 is approximated as (37), as shown at the bottom of the next page, where  $\tilde{\Xi}_P^{\frac{2}{\alpha}} = 2\left(1 + \frac{\tilde{\mu}_o \Pi_1}{\tilde{\mu}_1^{(a)}}\right)^{\frac{\mathcal{T}_t}{W_1}} - 1$ , and  $\tilde{\Xi}_{F,k}^{\frac{2}{\alpha}} = 2\left(\mathbb{1}_{\{k \in 0 \cup K\}} + \frac{\tilde{\mu}_o \Pi_k}{\tilde{\mu}_k^{(a)}}\right)^{\frac{\mathcal{T}_t}{W_k}} - 1$ .

## VI. NUMERICAL RESULTS

In this section, we evaluated some numerical results of the transmission probability and the network throughput, and give some interpretations based on our theoretical analysis. Unless otherwise specified, we set the transmission power of the UAVs is  $P_u = 20$  W, and the density is  $\mu_u = 5 \times 10^{-2}$  nodes/m<sup>2</sup>; path-loss exponent  $\alpha = 4$ , the energy harvesting efficiency  $\eta = 0.8$ , the transmission power of the MBSs and IoT-Ts is  $P_m = 43$  dBm, and  $P_1 = 20$  dBm, respectively. The target SIR  $\mathcal{T}_t = 256 \times 10^3$  bits/sec, the distance between the IoT-T and its associated IoT-D  $d_a = 5$  m, the probability that the IoT-Ds require communications  $\omega_{req} = 0.9$ , the density of the MBSs in tier 0 and the IoT-Ts in tier 1 is  $\mu_m = 10^{-6}$  nodes/m<sup>2</sup>, and  $\mu_1 = 2 \times 10^{-4}$  nodes/m<sup>2</sup>, respectively. The density of the ordinary IoT-Ds is  $\mu_o = 5 \times 10^{-4}$  nodes/m<sup>2</sup>, and the association biasing factor in tier 0 and 1 are  $\mathcal{A}_0 = 1$ , and  $\mathcal{A}_1 = 30$ , respectively. The height of the UAVs is  $h_{uav} = 4$  m.

### A. PERFORMANCE OF THE TRANSMISSION PROBABILITY

Fig. 5 shows the transmission probability of the IoT-Ts  $\omega_t$  versus the transmission power  $P_1$ , for different values of the communication request probability of an IoT-D  $\omega_{req}$ . It is observed that  $\omega_t$  is a fix value when  $0 \leq P_k \leq P_{slot}^{\min}$ , while  $P_{slot}^{\min} < P_k \leq 2P_{slot}^{\min}$ ,  $\omega_t$  is increasing with the transmission power  $P_1$ , which are consistent with the simulation results.

$$\begin{aligned} \mathcal{H}_c \\ = \left( \mathcal{T}_t \sum_{k=1}^K \omega_f \omega_{req} \mu_k \sum_{n=0}^{\infty} \exp \left( - \sum_{j=0}^K \tilde{\mu}_j^{(a)} \left( \Xi_t^{PAID}(num_k) \right)^{\frac{2}{\alpha}} d_{a,k}^2 \kappa(\alpha) \left( \frac{P_j}{P_k} \right)^{\frac{2}{\alpha}} \right) s_{num_k}(n) \right. \\ + \sum_{k=0}^K \sum_{n=1}^{\infty} \left[ \int_0^{\infty} 2\pi x \frac{\sum_{i=0}^K \mu_i^{(a)} (P_i \mathcal{A}_i)^{\frac{2}{\alpha}}}{(P_k \mathcal{A}_k)^{\frac{2}{\alpha}}} \exp \left( -\pi x^2 \sum_{j=0}^K \left( \frac{P_j}{P_k} \right)^{\frac{2}{\alpha}} \left( \tilde{\mu}_j^{(a)} \mathcal{M}\left(\Xi_t^{FAID}(num_k), \alpha, \frac{\mathcal{A}_j}{\mathcal{A}_k}\right) + \mu_j^{(a)} \left( \frac{\mathcal{A}_j}{\mathcal{A}_k} \right)^{\frac{2}{\alpha}} \right) \right) dx \right] \\ \times \mathcal{T}_t s_{num_k}(n) \Pi_k \times \left( \sum_{k=1}^K (1 - \omega_f) \cdot \omega_{req} \mu_k + \omega_{req} \cdot \mu_o \right) \Big) / (\mu_m (1 - s_{num_0}(0)) P_m + \omega_t \cdot \mu_1 P_1). \quad (35) \end{aligned}$$

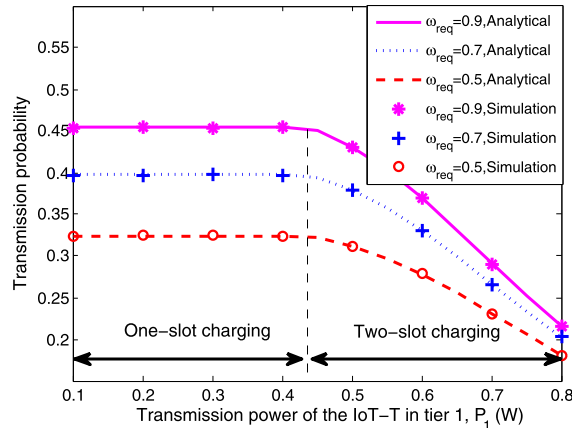


**FIGURE 5.** Transmission probability versus the transmission power of IoT-T in tier 1.

From (20) and (25), it can be observed that  $\omega_t$  has no relationship with  $P_1$  for one-slot charging, due to the fact that once an IoT-Ts located inside a harvesting zone, it can be ensured to be fully charged within one time slot; and for two-slot charging, increasing  $P_1$  resulting to a smaller region  $\mathfrak{R}_1$ , which means that most of the IoT-Ts need to be fully charged within two time slots, thus the probability  $\omega_f$  becomes smaller, and  $\omega_t$  becomes smaller, accordingly. Furthermore, with (20) and (25), we can easily obtain that  $\omega_t$  is increasing with the communication request probability of an IoT-D  $\omega_{req}$ .

Fig. 6 demonstrates how the density of the UAVs  $\mu_u$  and the transmission power of the IoT-Ts  $P_1$  would affect the transmission probability  $\omega_t$ . The observations are as follows. First, the effective of  $P_1$  is consistent with that in Fig. 5. Second, for a constant  $P_1$ ,  $\omega_t$  is firstly monotonically increasing with the density of the UAVs  $\mu_u$  and then converge to a constant as  $\mu_u$  increases, the reason is that the increased density of the UAV will cause more IoT-Ts to be fully charged for data transmission, and  $\omega_t$  will increase first, and when the density of the UAVs exceeds a threshold, the density of the active IoT-Ts will be saturated, thus  $\omega_t$  will remain stable and convergence to a fix value. The results can provide useful insights and guidelines for the UAV deployments in special areas.

## B. PERFORMANCE OF NETWORK THROUGHPUT AND ENERGY EFFICIENCY

Fig. 7 shows the network throughput given in (33) as a function of the density of the IoT-Ts,  $\mu_1$ , under different values of

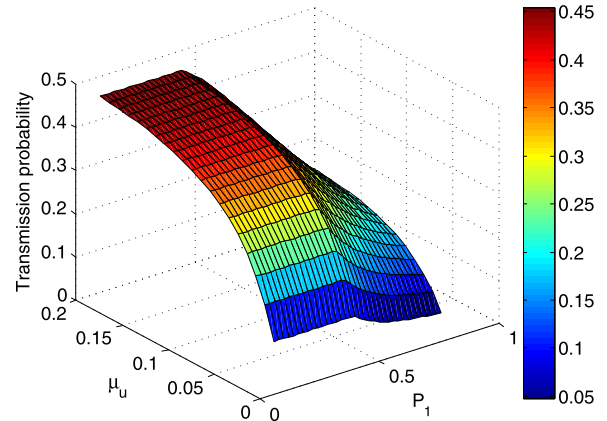


**FIGURE 6.** Transmission probability versus the density of UAVs and the transmission power of IoT-T in tier 1.

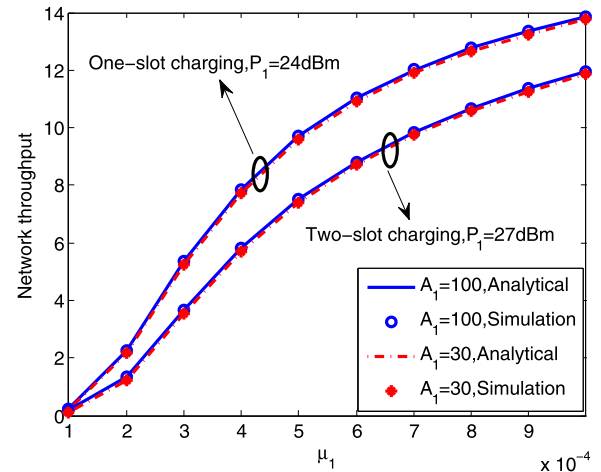


**FIGURE 7.** The network throughput versus the density of IoT-Ts in tier 1.

the transmission power  $P_1$ , and the association biasing factor  $\mathcal{A}_1$ . The observations are given as follows. First, the simulation curves are consistent with our analytical results for the different values of the density  $\mu_1$ ; Second, the network throughput is monotonically increasing with  $\mu_1$ , the reason is that as  $\mu_1$  increases, the number of FAIDs are increases due to the increase number of associated IoT-Ds whose IoT-Ts are inactive, accordingly, from (11), the density of active IoT-Ts that can be used for dividing the load increases. This can reduce the density of transmitting MBSs, which correspondingly leads to less interference from tier 0 to the IoT-Ds and higher network throughput. Third, for different transmission

$$\begin{aligned} \tilde{\mathcal{H}}_c = & \left( \mathcal{T}_t \omega_f \omega_{req} \mu_1 \exp \left( - \sum_{j=0}^1 \tilde{\mu}_j^{(a)} \tilde{\Xi}_P^{\frac{2}{\alpha}} d_a^2 \kappa(\alpha) \left( \frac{P_j}{P_1} \right)^{\frac{2}{\alpha}} \right) \right. \\ & + \sum_{k=0}^1 \int_0^\infty 2\pi x \mu_k^{(a)} \exp \left( -\pi x^2 \sum_{j=0}^1 \left( \frac{P_j}{P_k} \right)^{\frac{2}{\alpha}} \left( \tilde{\mu}_j^{(a)} \mathcal{M} \left( \tilde{\Xi}_{F,k}^{\frac{2}{\alpha}}, \alpha, \frac{\mathcal{A}_j}{\mathcal{A}_k} \right) + \mu_j^{(a)} \left( \frac{\mathcal{A}_j}{\mathcal{A}_k} \right)^{\frac{2}{\alpha}} \right) \right) dx \\ & \times \mathcal{T}_t ((1 - \omega_f) \cdot \omega_{req} \mu_1 + \omega_{req} \cdot \mu_o) / (\mu_m (1 - s_{num_0}(0)) P_m + \omega_t \cdot \mu_1 P_1). \end{aligned} \quad (37)$$

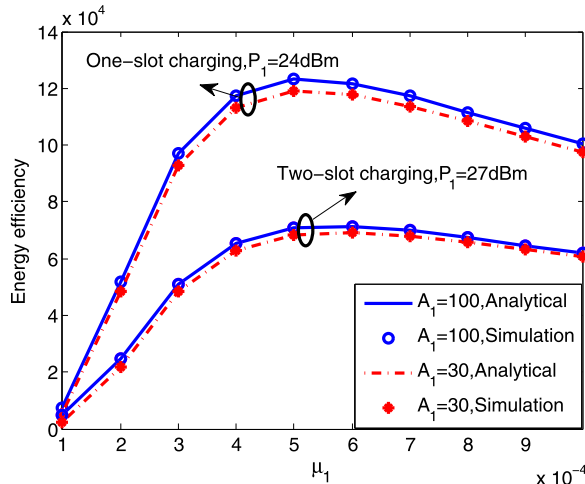


**FIGURE 8.** The energy efficiency versus the density of IoT-Ts in tier 1.

power  $P_1$ , there are two cases to be analyzed, which is one-slot charging ( $P_1 = 24$  dBm), and two-slot charging ( $P_1 = 27$  dBm). Compare with two-slot charging, the IoT-Ts that located in the UAV's harvesting zone can be fully charged within one time slots with one-slot charging, thus result in a higher probability  $\omega_t$  and  $\Pi_1$ , and most IoT-Ds will connect to tier 1, which can similarly leads to less interference from tier 0 to the IoT-Ds and higher network throughput. Furthermore, it is also observed that choosing a larger association biasing factor in tier 1,  $A_1 = 100$ , which means that associating most IoT-Ds to tier 1, can improve the network throughput.

Fig. 8 shows the energy efficiency given in (35) as a function of the density of the IoT-Ts,  $\mu_1$ , under different

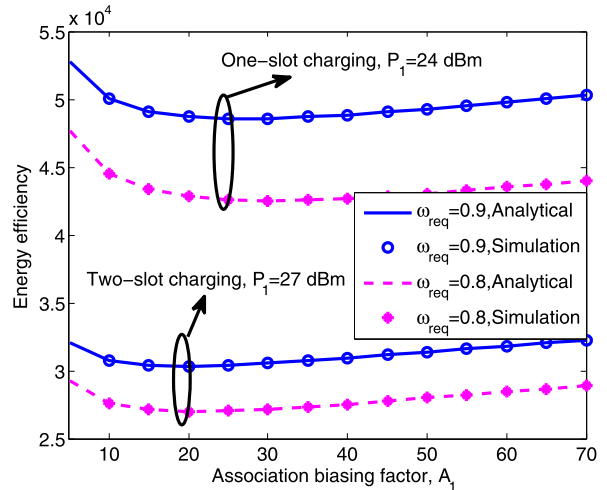


**FIGURE 9.** The energy efficiency versus the association biasing factor in tier 1.

values of the transmission power  $P_1$ , and the association biasing factor  $A_1$ . The observations are given as follows. The energy efficiency is firstly increasing with the density  $\mu_1$ , and then beginning to degrade when  $\mu_1$  exceeds a threshold. The reason is that as  $\mu_1$  increases, the network throughput correspondingly increases as shown in Fig. 7. However, the energy consumption is also continue to increase with  $\mu_1$ . Once  $\mu_1$  exceeds a threshold, the number of the MBs that in sleep mode is saturated, and the number of active IoT-Ts is continue to increase, the growing energy consumption cannot continue to maintain the increasing energy efficiency, and thus will be decreased. Moreover, reducing the transmission power

$$\begin{aligned}
 \Psi_{cov,k}^{PAID} &= \mathbb{E} \left[ \Pr \left( SIR_k^{PAID} \geq \Xi_t^{PAID} (\text{num}_k) \right) | \text{num}_k \right] \\
 &= \mathbb{E} \left[ \Pr \left( \frac{P_k g_{x_0,y_{k,0}} d_{a,k}^{-\alpha}}{\sum_{j=0}^K \sum_{i \in \tilde{\Phi}_j^{(a)} \setminus y_{k,0}} P_j g_{x_0,y_{j,i}} \|y_{j,i} - x_0\|^{-\alpha}} \geq \Xi_t^{PAID} (\text{num}_k) \right) | \text{num}_k \right] \\
 &= \mathbb{E} \left[ \Pr \left( g_{x_0,y_{k,0}} \geq \frac{\sum_{j=0}^K \sum_{i \in \tilde{\Phi}_j^{(a)} \setminus y_{k,0}} P_j g_{x_0,y_{j,i}} \|y_{j,i} - x_0\|^{-\alpha}}{P_k d_{a,k}^{-\alpha}} \Xi_t^{PAID} (\text{num}_k) \right) | \text{num}_k \right] \\
 &\stackrel{(a)}{=} \mathbb{E} \left[ \mathbb{E} \left[ \exp \left( -\frac{\Xi_t^{PAID} (\text{num}_k)}{P_k d_{a,k}^{-\alpha}} \sum_{j=0}^K I_j \right) | I_j \right] | \text{num}_k \right] \\
 &= \mathbb{E} \left[ \mathbb{E} \left[ \prod_{j=0}^K \exp \left( -\frac{\Xi_t^{PAID} (\text{num}_k)}{P_k d_{a,k}^{-\alpha}} I_j \right) | I_j \right] | \text{num}_k \right] \\
 &= \sum_{n=0}^{\infty} \mathbb{E}_{I_j} \left[ \prod_{j=0}^K \exp \left( -\frac{\Xi_t^{PAID} (\text{num}_k)}{P_k d_{a,k}^{-\alpha}} I_j \right) \right] s_{\text{num}_k}(n).
 \end{aligned} \tag{38}$$

$P_1$  is satisfying to improve the energy efficiency, this can be explained as that smaller  $P_1$  is associated with one-slot charging, which results to a higher density of active IoT-Ts. Finally, choosing a larger association biasing factor in tier 1  $\mathcal{A}_1 = 100$  can enhance the energy efficiency, which is consistent with the trend of the network throughput.

Fig. 9 demonstrates the energy efficiency as a function of the association biasing factor in tier 1  $\mathcal{A}_1$ . We have the following observations. The energy efficiency is initially decreases with small  $\mathcal{A}_1$  due to the overloading of the data in tier 1, the coverage probability of the PAIDs and FAIDs are both decreasing with  $\mathcal{A}_1$ , thus result to the degrade of the energy efficiency; As  $\mathcal{A}_1$  become larger, the energy efficiency starts to increase since the number of active MBSs are decreased, thus the interference from MBSs to the IoT-Ds is decreasing. However, the increase will be diminish and the energy efficiency converges to a fixed value, the reason is that all the IoT-Ds will be offloaded to tier 1 as the increase of  $\mathcal{A}_1$ , and all the MBSs will eventually become sleep mode state. Furthermore, larger  $\omega_{req}$  will result in a larger  $\omega_t$ , and more IoT-Ds can be served, thus result to a larger energy efficiency.

## VII. CONCLUSION

In this paper, we investigate a UAV-assisted downlink heterogeneous IoT system consisting of macrocells and IoT-Ts with energy harvesting. The transmission probability of the energy-constrained IoT-Ts is derived by considering one-slot and two-slot charging, and the PPP models for the 3D spatial distributions of the UAV swarms, MBSs, and IoT-Ts. Energy efficiency is maximized by optimizing the IoT-T density. The network throughput and energy efficiency are

both characterized by considering the effect of the association biasing factor, and the transmission power of the active IoT-Ts. The results can provide insightful guideline on the network parameters and the deployment for practical UAV swarms and IoT system.

## APPENDIX A PROOF OF RESULT 1

From (27), we derive the coverage probability of a PAIDs that is served by its associated IoT-T in tier- $k$  as (38), as shown at the bottom of the previous page.

The (a) in (38) follows from

$$I_j = \sum_{i \in \tilde{\Phi}_j^{(a)} \setminus \mathbb{V}_{k,0}} P_j g_{x_0, y_{j,i}} \|y_{j,i} - x_0\|^{-\alpha}. \quad (39)$$

Note that  $\mathbb{E}_{I_j} \left[ \exp \left( -\frac{\Xi_t^{PAID}(\text{num}_k)}{P_k d_{a,k}^{-\alpha}} I_j \right) \right]$  are Laplace transforms of the random variables  $I_j$ , with input parameter  $\frac{\Xi_t^{PAID}(\text{num}_k)}{P_k d_{a,k}^{-\alpha}}$ . According to the result in [37], the Laplace transform of the random variables  $I_j$  is obtained by

$$\begin{aligned} & \mathcal{L}_{I_j} \left( \frac{\Xi_t^{PAID}(\text{num}_k)}{P_k d_{a,k}^{-\alpha}} \right) \\ &= \exp \left( -\tilde{\mu}_j^{(a)} \left( \Xi_t^{PAID}(\text{num}_k) \right)^{\frac{2}{\alpha}} d_{a,k}^2 \kappa \left( \frac{P_j}{P_s} \right)^{\frac{2}{\alpha}} \right). \end{aligned} \quad (40)$$

Putting (40) into (38), and combining with (13), the coverage probability of a PAIDs that is served by its associated IoT-T in tier- $k$  is obtained after some algebraic calculation. This completes the proof of Result 1.

$$\begin{aligned} \Psi_{cov,k}^{FAID} &= \mathbb{E} \left[ \Pr \left( \frac{P_k g_{x'_0, y'_{k,0}} x^{-\alpha}}{\sum_{j=0}^K \sum_{i \in \tilde{\Phi}_j^{(a)} \setminus \mathbb{V}'_{k,0}} P_j g_{x'_0, y'_{j,i}} \|y'_{j,i} - x'_0\|^{-\alpha}} \geq \Xi_t^{FAID}(\text{num}_k) \right) | \text{num}_k \right] \\ &= \mathbb{E} \left[ \Pr \left( g_{x'_0, y'_{k,0}} \geq \frac{\sum_{j=0}^K \sum_{i \in \tilde{\Phi}_j^{(a)} \setminus \mathbb{V}'_{k,0}} P_j g_{x'_0, y'_{j,i}} \|y'_{j,i} - x'_0\|^{-\alpha}}{P_k x^{-\alpha}} \Xi_t^{FAID}(\text{num}_k) \right) | \text{num}_k \right] \\ &= \mathbb{E} \left[ \mathbb{E} \left[ \exp \left( -\frac{\Xi_t^{FAID}(\text{num}_k)}{P_k x^{-\alpha}} \sum_{j=0}^K I'_j \right) | I'_j \right] | \text{num}_k \right] \\ &= \int_0^\infty \mathbb{E} \left[ \mathbb{E}_{I'_j} \left[ \prod_{j=0}^K \exp \left( -\frac{\Xi_t^{FAID}(\text{num}_k)}{P_k x^{-\alpha}} I'_j \right) \right] | \text{num}_k \right] s_{X_k}(x) dx \\ &= \sum_{n=1}^\infty \left[ \int_0^\infty \prod_{j=0}^K \mathcal{L}_{I'_j} \left( \frac{\Xi_t^{FAID}(\text{num}_k)}{P_k x^{-\alpha}} \right) s_{X_k}(x) dx \right] s_{\text{num}_k}(n). \end{aligned} \quad (41)$$

## APPENDIX B

### PROOF OF RESULT 2

We derive the coverage probability  $\Psi_{cov,k}^{PAID}$  as follows, starting with the  $SIR_k^{FAID}$  given in (30). We have (41), as shown at the bottom of the previous page.

Using the same method as the proof Result 1, and as mentioned before, the total interference of a typical FAID received is from all IoT-Ts or MBSs in tier  $i$  which are located out of a circle centered at the typical FAID with radius  $d_j = x \left( \frac{P_i A_i}{P_k A_k} \right)^{-\alpha}$ . Then, we have

$$\begin{aligned} & \mathcal{L}_{I_j} \left( \frac{\Xi_t^{FAID}(\text{num}_k)}{P_k x^{-\alpha}} \right) \\ &= \exp \left( -\pi \tilde{\mu}_j^{(a)} \left( \frac{P_j}{P_k} \right)^{\frac{2}{\alpha}} \mathcal{M} \left( \Xi_t^{FAID}(\text{num}_k), \alpha, \frac{A_j}{A_k} \right) x^2 \right). \end{aligned} \quad (42)$$

where  $\mathcal{M} \left( \Xi_t^{FAID}(\text{num}_k), \alpha, \frac{A_j}{A_k} \right)$  is given by (32). Putting (12) and (42) into (41),  $\Psi_{cov,k}^{PAID}$  can be obtained. This completes the proof of Result 2.

## REFERENCES

- [1] S. Cho, K. Lee, B. Kang, K. Koo, and I. Joe, "Weighted harvest-then-transmit: UAV-enabled wireless powered communication networks," *IEEE Access*, vol. 6, pp. 72212–72224, 2018.
- [2] J. Zhang, S. Chen, R. G. Maunder, R. Zhang, and L. Hanzo, "Regularized zero-forcing precoding-aided adaptive coding and modulation for large-scale antenna array-based air-to-air communications," *IEEE J. Sel. Areas Commun.*, vol. 36, no. 9, pp. 2087–2103, Sep. 2018.
- [3] J. Zhang, T. Chen, S. Zhong, J. Wang, W. Zhang, X. Zuo, R. G. Maunder, and L. Hanzo, "Aeronautical *ad hoc* networking for the Internet-above-the-clouds," *Proc. IEEE*, vol. 107, no. 5, pp. 868–911, May 2019.
- [4] L. Xie, J. Xu, and R. Zhang, "Throughput maximization for UAV-enabled wireless powered communication networks," *IEEE Internet Things J.*, vol. 6, no. 2, pp. 1690–1703, Apr. 2019.
- [5] F. Huang, J. Chen, H. Wang, G. Ding, Y. Gong, and Y. Yang, "Multiple-UAV-assisted SWIPT in Internet of Things: User association and power allocation," *IEEE Access*, vol. 7, pp. 124244–124255, 2019.
- [6] F. Huang, J. Chen, H. Wang, G. Ding, Z. Xue, Y. Yang, and F. Song, "UAV-assisted SWIPT in Internet of Things with power splitting: Trajectory design and power allocation," *IEEE Access*, vol. 7, pp. 68260–68270, 2019.
- [7] C. Yan, L. Fu, J. Zhang, and J. Wang, "A comprehensive survey on UAV communication channel modeling," *IEEE Access*, vol. 7, pp. 107769–107792, 2019.
- [8] Z. Xue, J. Wang, G. Ding, and Q. Wu, "Joint 3D location and power optimization for UAV-enabled relaying systems," *IEEE Access*, vol. 6, pp. 43113–43124, 2018.
- [9] J.-K. Zhang, S. Chen, R. G. Maunder, R. Zhang, and L. Hanzo, "Adaptive coding and modulation for large-scale antenna array-based aeronautical communications in the presence of co-channel interference," *IEEE Trans. Wireless Commun.*, vol. 17, no. 2, pp. 1343–1357, Feb. 2018.
- [10] C. Xu, T. Bai, J. Zhang, R. Rajashekhar, R. G. Maunder, Z. Wang, and L. Hanzo, "Adaptive coherent/non-coherent spatial modulation aided unmanned aircraft systems," *IEEE Wireless Commun.*, vol. 26, no. 4, pp. 170–177, May 2019.
- [11] Y. Zeng, R. Zhang, and T. J. Lim, "Wireless communications with unmanned aerial vehicles: Opportunities and challenges," *IEEE Commun. Mag.*, vol. 54, no. 5, pp. 36–42, May 2016.
- [12] H. Wang, G. Ding, F. Gao, J. Chen, J. Wang, and L. Wang, "Power control in UAV-supported ultra dense networks: Communications, caching, and energy transfer," *IEEE Commun. Mag.*, vol. 56, no. 6, pp. 28–34, Jun. 2018.
- [13] Y. Zeng and R. Zhang, "Energy-efficient UAV communication with trajectory optimization," *IEEE Trans. Wireless Commun.*, vol. 16, no. 6, pp. 3747–3760, Jun. 2017.
- [14] Z. Zhu, S. Huang, Z. Chu, F. Zhou, D. Zhang, and I. Lee, "Robust designs of beamforming and power splitting for distributed antenna systems with wireless energy harvesting," *IEEE Syst. J.*, vol. 13, no. 1, pp. 30–41, Mar. 2019.
- [15] Y. Wang, M. Hua, Z. Liu, D. Zhang, B. Ji, and H. Dai, "UAV-based mobile wireless power transfer systems with joint optimization of user scheduling and trajectory," *Mobile Netw. Appl.*, pp. 1–15, 2019.
- [16] Z. Chu, Z. Zhu, and J. Hussein, "Robust optimization for AN-Aided transmission and power splitting for secure MISO SWIPT system," *IEEE Commun. Lett.*, vol. 20, no. 8, pp. 1571–1574, Aug. 2016.
- [17] Z. Chu, F. Zhou, P. Xiao, Z. Zhu, D. Mi, N. Al-Dhahir, and R. Tafazolli, "Resource allocation for secure wireless powered integrated multicast and unicast services with full duplex self-energy recycling," *IEEE Trans. Wireless Commun.*, vol. 18, no. 1, pp. 620–636, Jan. 2019.
- [18] X. Lu, P. Wang, D. Niyato, D. I. Kim, and Z. Han, "Wireless charging technologies: Fundamentals, standards, and network applications," *IEEE Commun. Surveys Tuts.*, vol. 18, no. 2, pp. 1413–1452, 2nd Quart., 2016.
- [19] Z. Zhu, Z. Chu, F. Zhou, H. Niu, Z. Wang, and I. Lee, "Secure beamforming designs for secrecy MIMO SWIPT systems," *IEEE Wireless Commun. Lett.*, vol. 7, no. 3, pp. 424–427, Jun. 2018.
- [20] Z. Zhu, Z. Chu, Z. Wang, and I. Lee, "Outage constrained robust beamforming for secure broadcasting systems with energy harvesting," *IEEE Trans. Wireless Commun.*, vol. 15, no. 11, pp. 7610–7620, Nov. 2016.
- [21] X. Pan, C. Yan, and J. Zhang, "Nonlinearity-based single-channel monopulse tracking method for OFDM-aided UAV A2G communications," *IEEE Access*, vol. 7, pp. 148485–148494, 2019.
- [22] Z. Xue, J. Wang, G. Ding, H. Zhou, and Q. Wu, "Maximization of data dissemination in UAV-supported Internet of Things," *IEEE Wireless Commun. Lett.*, vol. 8, no. 1, pp. 185–188, Feb. 2019.
- [23] M. Mozaffari, W. Saad, M. Bennis, and M. Debbah, "Mobile unmanned aerial vehicles (UAVs) for energy-efficient Internet of Things communications," *IEEE Trans. Wireless Commun.*, vol. 16, no. 11, pp. 7574–7589, Nov. 2017.
- [24] W. Feng, J. Wang, Y. Chen, X. Wang, N. Ge, and J. Lu, "UAV-aided MIMO communications for 5G Internet of Things," *IEEE Internet Things J.*, vol. 6, no. 2, pp. 1731–1740, Apr. 2019.
- [25] J. Xu, Y. Zeng, and R. Zhang, "UAV-enabled wireless power transfer: Trajectory design and energy region characterization," in *Proc. IEEE Globecom Workshops (GC Wkshps)*, Singapore, Dec. 2017, pp. 1–7.
- [26] M. Li, W. Yang, X. Yi, Y. Wang, and J. Wang, "Swarm robot task planning based on air and ground coordination for disaster search and rescue," *J. Mater. Eng.*, vol. 55, no. 11, pp. 1–9, Jun. 2019.
- [27] Y. Liu, Z. Qin, Y. Cai, Y. Gao, G. E. Li, and A. Nallanathan, "UAV communications based on non-orthogonal multiple access," Sep. 2018, arXiv:1809.05767. [Online]. Available: <https://arxiv.org/abs/1809.05767>
- [28] D. Stoyan, W. Kendall, and J. Mecke, *Stochastic Geometry and Its Applications*, 2nd ed. Hoboken, NJ, USA: Wiley, 1996.
- [29] F. Baccelli and B. Blaszczyszyn, "Stochastic geometry and wireless networks: Volume II applications," in *Foundations and Trends in Networking*, vol. 4, nos. 1–2, pp. 1–312, 2010.
- [30] A. Al-Hourani, S. Kandeepan, and S. Lardner, "Optimal LAP altitude for maximum coverage," *IEEE Wireless Commun. Lett.*, vol. 3, no. 6, pp. 569–572, Dec. 2014.
- [31] S. Lee, R. Zhang, and K. Huang, "Opportunistic wireless energy harvesting in cognitive radio networks," *IEEE Trans. Wireless Commun.*, vol. 12, no. 9, pp. 4788–4799, Sep. 2013.
- [32] X. Song, C. Yin, D. Liu, and R. Zhang, "Spatial throughput characterization in cognitive radio networks with threshold-based opportunistic spectrum access," *IEEE J. Sel. Areas Commun.*, vol. 32, no. 11, pp. 2190–2204, Nov. 2014.
- [33] Y. Yao, X. Chen, X. Li, and X. Song, "Hybrid small cell base station deployment in heterogeneous cellular networks with wireless power transfer," *Inf. Sci.*, no. 454, pp. 16–29, Jul. 2018.
- [34] P.-S. Yu, J. Lee, T. Q. S. Quek, and Y.-W. P. Hong, "Traffic offloading in heterogeneous networks with energy harvesting personal cells-network throughput and energy efficiency," *IEEE Trans. Wireless Commun.*, vol. 15, no. 2, pp. 1146–1161, Feb. 2016.
- [35] S. Singh, H. S. Dhillon, and J. G. Andrews, "Offloading in heterogeneous networks: Modeling, analysis, and design insights," *IEEE Trans. Wireless Commun.*, vol. 12, no. 5, pp. 2484–2497, May 2013.

- [36] H.-S. Jo, Y. J. Sang, P. Xia, and J. G. Andrews, "Heterogeneous cellular networks with flexible cell association: A comprehensive downlink SINR analysis," *IEEE Trans. Wireless Commun.*, vol. 11, no. 10, pp. 3484–3495, Oct. 2012.
- [37] M. Haenggi, J. G. Andrews, F. Baccelli, O. Dousse, and M. Franceschetti, "Stochastic geometry and random graphs for the analysis and design of wireless networks," *IEEE J. Sel. Areas Commun.*, vol. 27, no. 7, pp. 1029–1046, Sep. 2009.



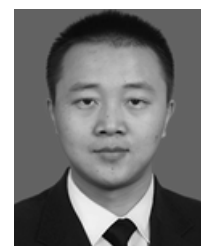
**YUANYUAN YAO** received the Ph.D. degree in information and communication engineering from the Beijing University of Posts and Telecommunications, Beijing, China, in 2017. Since 2017, she has been with the School of Information and Communication Engineering, Beijing Information Science and Technology University, Beijing, as an Associate Professor. Her research interests include stochastic geometry and its applications in large-scale wireless networks, energy harvesting, and wireless communication.



**ZHENGYU ZHU** received the B.S. degree from Henan University, in 2010, and the Ph.D. degree from Zhengzhou University, China, in 2017. He is currently with the School of Information Engineering, Zhengzhou University, and with the Zhengzhou University Research Institute of Industrial Technology Company Ltd., Zhengzhou, China. His research interests include information theory and signal processing for wireless communications, such as MIMO wireless networks, physical layer security, wireless cooperative networks, convex optimization techniques, and energy harvesting communication systems.



**SAI HUANG** is currently working with the Department of Information and Communication Engineering, Beijing University of Posts and Telecommunications, as a Lecturer. He serves as an Academic Secretary with the Key Laboratory of Universal Wireless Communications, Ministry of Education, China. He is the Reviewer of international journals, such as the IEEE TRANSACTIONS ON VEHICULAR TECHNOLOGY, the IEEE WIRELESS COMMUNICATIONS LETTERS, the IEEE TRANSACTIONS ON COGNITIVE COMMUNICATIONS AND NETWORKING and the international conferences, such as IEEE ICC and IEEE GLOBECOM. His research directions are machine learning assisted intelligent signal processing, statistical spectrum sensing and analysis, fast detection and depth recognition of universal wireless signals, millimeter wave signal processing, and cognitive radio networks.



**XINWEI YUE** received the degree from the Yellow River Conservancy Technical Institute, in 2007, the M.S. degree from Henan Normal University, in 2013, and the Ph.D. degree in communication and information system from Beihang University (BUAA), Beijing, in 2018. He has been a Lecture with the School of Information and Communication Engineering, Beijing Information Science and Technology University (BISTU), Beijing, since 2018, and promoted to Associate Professor, in 2019. His research interests include 5G/6G networks, wireless communications theory, non-orthogonal multiple access, cooperative networks, and physical layer security.



**CHUNYU PAN** received the Ph.D. degree with the School of Information and Communication Engineering, Beijing University of Posts and Telecommunications, Beijing, China. She has been a Lecturer with the School of Information and Communication Engineering, Beijing Information Science and Technology University, Beijing, since July 2019. Her research interests include software-defined cellular networks, heterogeneous wireless networks, resource allocation and mobility management in cellular networks.



**XUEHUA LI** received the Ph.D. degree in telecommunications engineering from the Beijing University of Posts and Telecommunications, Beijing, China, in 2008. She is currently a Professor and the Deputy Dean of the School of Information and Communication Engineering with the Beijing Information Science and Technology University, Beijing. She is also a Senior Member of the Beijing Internet of Things Institute. Her research interests are in the broad areas of communications and information theory, particularly the Internet of Things, and coding for multimedia communications systems.